J. Phys.: Condens. Matter **23** (2011) 156003 (4pp) doi:10.1088/0953-8984/23/15/156003

Room temperature antiferromagnetic order in superconducting $X_yFe_{2-x}Se_2$ (X = Rb, K): a neutron powder diffraction study

V Yu Pomjakushin[1], E V Pomjakushina[2], A Krzton-Maziopa[2], K Conder[2] and Z Shermadini[3]

[1] Laboratory for Neutron Scattering, Paul Scherrer Institut, CH-5232 Villigen PSI, Switzerland
[2] Laboratory for Developments and Methods, Paul Scherrer Institut, CH-5232 Villigen PSI, Switzerland
[3] Laboratory for Muon-Spin Spectroscopy, Paul Scherrer Institut, CH-5232 Villigen PSI, Switzerland

E-mail: Vladimir.Pomjakushin@psi.ch

Received 16 February 2011, in final form 9 March 2011
Published 1 April 2011
Online at stacks.iop.org/JPhysCM/23/156003

Abstract

Magnetic and crystal structures of superconducting $X_yFe_{2-x}Se_2$ (X = Rb and K with $T_c = 31.5$ and 29.5 K) have been studied by neutron powder diffraction at room temperature. Both crystals show an ordered iron vacancy pattern and the crystal structure is well described by the $I4/m$ space group with the lattice constants $a = 8.799$, $c = 14.576$ and $a = 8.730$, $c = 14.115$ Å and the refined stoichiometry $x = 0.30(1)$, $y = 0.83(2)$ and $x = 0.34(1)$, $y = 0.83(1)$ for Rb and K crystals, respectively. The structure contains one fully occupied iron position and one almost empty vacancy position. Assuming that the iron moment is ordered only on the fully occupied site we have sorted out all eight irreducible representations (irreps) for the propagation vector $k = 0$ and have found that irreps τ_2 and τ_7 fit the experimental data well with the moments along the c axis. The moment amplitudes amounted to 2.15(3) μ_B, 2.55(3) μ_B for τ_2 and 2.08(6) μ_B, 2.57(3) μ_B for τ_7 for Rb and K crystals, respectively. Irrep τ_2 corresponds to the Shubnikov group $I4/m'$ and gives a constant moment antiferromagnetic configuration, whereas τ_7 does not have a Shubnikov counterpart and allows two different magnetic moments in the structure.

(Some figures in this article are in colour only in the electronic version)

1. Introduction

The recent discovery of the Fe-based superconductors has triggered a remarkable renewed interest for possible new routes leading to high-temperature superconductivity. As observed in the cuprates, the iron-based superconductors exhibit interplay between magnetism and superconductivity, suggesting the possible occurrence of unconventional superconducting states. Other common properties are the layered structure and the low carrier density. Among the iron-based superconductors FeSe has the simplest structure with layers, in which Fe cations are tetrahedrally coordinated by Se [1]. Recently superconductivity at about 30 K was found in $X_yFe_{2-x}Se_2$ for X = K, Cs and Rb [2–5]. Muon-spin rotation/relaxation (μSR) experiments show that the superconducting state observed in $Cs_yFe_{2-x}Se_2$ below 28.5(2) K microscopically coexists with a magnetic phase with a transition temperature at $T_m = 478.5(3)$ K [6]. Recently the ~~atomic force microscope~~ (AFM) order was reported in superconducting $K_{0.8}Fe_{1.6}Se_2$ with $T_N = 560$ K with the iron magnetic moment 3.31 μ_B [7], and $Cs_yFe_{2-x}Se_2$ with the magnetic moment about 2 μ_B per iron site [8]. In the latter paper several possible symmetry adapted magnetic configurations have been proposed, including one with non-constant moment configuration. During the preparation of the

antifer
romag
netic

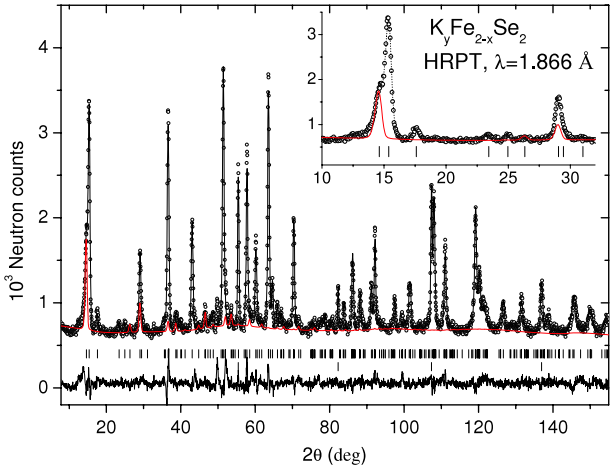

Figure 1. The Rietveld refinement pattern and difference plot of the neutron diffraction data for $K_yFe_{2-x}Se_2$ at room temperature ($T = 300$ K) measured at HRPT with the wavelength $\lambda = 1.886$ Å. The rows of ticks show the Bragg peak positions for the main phase and Fe impurity. The magnetic contribution together with the background is shown by a red line. The inset shows the zoomed low 2θ domain.

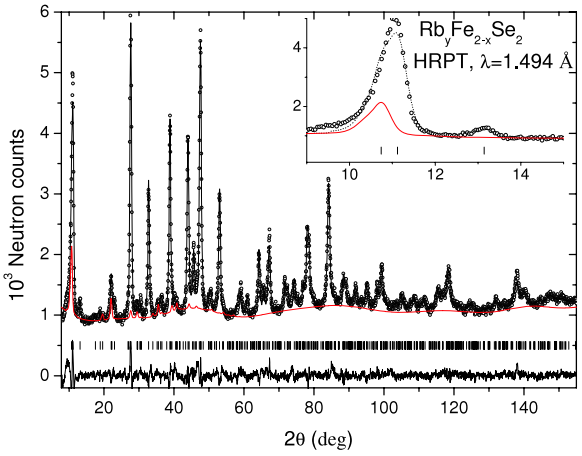

Figure 2. The Rietveld refinement pattern and difference plot of the neutron diffraction data for $Rb_yFe_{2-x}Se_2$ at room temperature ($T = 300$ K) measured at HRPT with the wavelength $\lambda = 1.494$ Å. The row of ticks shows the Bragg peak positions. The magnetic contribution together with the background is shown by a red line. The inset shows the zoomed low 2θ domain.

present paper, a new paper appeared confirming the AFM order in Cs crystals and reporting on the similar AFM structure in Rb crystals with the moment 1.9(2) μ_B [9].

The average crystal structure of $X_yFe_{2-x}Se_2$ is the same as in the layered (122-type) iron pnictides with the space group $I4/mmm$ [10]. Different types of iron vacancy ordering in $Tl_yFe_{2-x}Se_2$ were observed a long time ago [11–13], including one with a unit cell that is five times larger. Due to renewed interest in the superconducting chalcogenides many new experimental studies on the vacancy ordering in $X_yFe_{2-x}Se_2$(X = K, Tl) have appeared very recently [14–17, 7]. In the previous paper [8] we have determined the iron vacancy superstructure with k-vector star $\{[\frac{2}{5}, \frac{1}{5}, 1]\}$ in $Cs_yFe_{2-x}Se_2$ by means of single-crystal x-ray reciprocal space mapping and proposed two symmetry adapted magnetic configurations for the superstructure with $I4/m$ space group, that well fitted the powder neutron diffraction data combined with the single-crystal dataset. The coexistence of the superconductivity and the magnetic order with an extraordinary high Néel temperature is very unusual and the direct proof of the presence of the long range AFM ordering and the determination of the magnetic configurations by means of neutron diffraction seem to be very important. In this paper we report on the room temperature crystal and magnetic structures in the vacancy ordered superconducting $X_yFe_{2-x}Se_2$ (X = Rb, K).

2. Samples: experimental details

Single crystals of intercalated iron selenides of nominal compositions $X_{0.8}(FeSe_{0.98})_2$ were grown from the melt using the Bridgman method as described in [3]. The superconducting transition has been detected by ac susceptibility using a conventional magnetometer. The sample holder contains a standard coil system with a primary excitation coil (1300 windings, 40 mm long) and two counter-wound pick-up coils (reference and sample coil, each 10 mm long and 430 windings) which are connected to a lock-in amplifier. The frequency used was 144 Hz and the sample holder diameter was 5 mm. Measurements were performed by heating the sample at a rate of 9 K h^{-1}. The onset of the critical temperature has been determined to be $T_c = 31.5$ K and 29.5 K for the Rb and K intercalated compounds, respectively. The magnetometer was calibrated using the superconducting transition of a lead sample showing a 100% superconducting fraction. The raw data were then normalized to the sample volume relative to that of the Pb calibration specimen. The superconducting fraction determined this way amounted to 73–100% and 22% for the Rb and K crystals, respectively. Neutron powder diffraction experiments were carried out at the SINQ spallation source of the Paul Scherrer Institute (Switzerland) using the high-resolution diffractometer for thermal neutrons HRPT [18] ($\lambda = 1.866, 1.494$ Å, high intensity mode $\Delta d/d \geqslant 1.8 \times 10^{-3}$) at room temperature. For the powder diffraction measurements pieces of the corresponding crystal were powdered and loaded into a vanadium container with an indium seal in a He glove box. Inasmuch as the K-containing sample was measured just after the first successful synthesis, we were not aware that the tip of the crystal taken from the Bridgman ampoule always contains impurity phases (predominantly Fe) and we have measured a mixture of precipitated impurities together with powdered crystal. As for the Rb crystal we have powdered only the middle part of the crystal, which looked like a single domain with a shiny surface. Refinement of crystal and magnetic structures of the powder neutron diffraction data were carried out using the FULLPROF [19] program, with the use of its internal tables for scattering lengths and magnetic form factors.

Table 1. Crystal and magnetic structure parameters of $X_yFe_{2-x}Se_2$ (X = Rb, K) refined in the space group $I4/m$ (no. 87) with the atoms in the Wyckoff positions: X1 (0, 0, 0) (2a), X2 (x, y, 0) (8h), Se1 in (x, y, z) (16i), Se2 ($\frac{1}{2}$, $\frac{1}{2}$, z) (4e), Fe2 (16i) and Fe1 ($\frac{1}{2}$, 0, $\frac{1}{4}$) (4d). The occupancies o-X, o-Fe are calculated to be in units of the formula $X_yFe_{2-x}Se_2$. The occupancy of Fe2 was fixed to the fully occupied value, which corresponds to stoichiometry 1.6. Atomic displacement parameters B (Å^2) were constrained to be the same for the same atom types. χ^2 is the global chi-square (Bragg contribution). Reliability Bragg R_B factors are given for the nuclear and magnetic phases, respectively. For $K_yFe_{2-x}Se_2$ we have performed a combined refinement of two datasets measured with wavelengths $\lambda_1 = 1.494$ Å and $\lambda_2 = 1.866$ Å. The magnetic moment amplitudes are in μ_B. The magnetic configurations for two magnetic models (τ_2, τ_7) that fit the data equally well are shown in figure 4. τ_4 fits the data considerably worse, but is given in the table for comparison.

	Rb	K
a	8.79962(24)	8.73019(12)
c	14.57615(53)	14.11485(30)
x, y X2	0.399(3) 0.803(3)	0.374(3) 0.816(5)
o-X1	0.59(2)	0.60(1)
o-X2	0.24(2)	0.23(1)
B X	3.9(1)	2.2(3)
x, y, z Se1	0.3880(9) 0.794(1)	0.3867(8) 0.795(1)
	0.6495(3)	0.6448(3)
z Se2	0.145(1)	0.142(1)
B Se	1.57(6)	1.43(6)
x, y, z Fe2	0.2958(8) 0.5920(8)	0.2953(8) 0.5914(6)
	0.2524(8)	0.2495(9)
o-Fe1	0.099(6)	0.069(6)
B Fe	1.79(6)	1.55(5)
τ_2		
$m \parallel c$ Fe2	2.15(6)	2.55(3)
χ^2	2.78	2.18
R_B,% λ_1	5.36 12.7	6.13 7.58
R_B,% λ_2		5.62 10.3
τ_7, τ_5		
$m \parallel c$ Fe2	2.08(6)	2.57(3)
χ^2	2.80	2.20
R_B,% λ_1	5.36 13.4	6.17 8.69
R_B,% λ_2		5.64 12.2
τ_4		
$m \perp c$ Fe2	1.71(6)	2.46(4)
χ^2	2.92	2.56
R_B,% λ_1	5.91 16.5	6.81 19.1
R_B,% λ_2		6.32 23.5

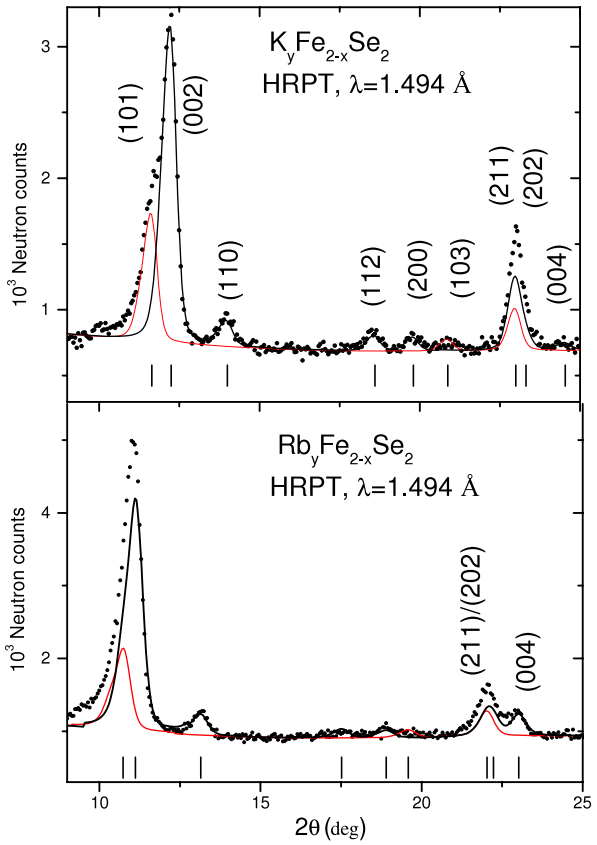

Figure 3. Fragments of NPD patterns for $X_yFe_{2-x}Se_2$ (X = K, Rb) at room temperature for $\lambda = 1.494$ Å and the partial magnetic and nuclear contributions shown by red and black lines. The row of ticks shows the Bragg peak positions.

3. Results and discussion

Figure 1 shows the neutron powder diffraction pattern (NPD) and the calculated profile for $K_yFe_{2-x}Se_2$. The refinement of the data was performed using two NPD datasets collected at different wavelengths $\lambda = 1.866$ and 1.494 Å. This allows one to have better resolution for the magnetic reflections from longer λ and better determination of the crystal structure parameters from the shorter wavelength. Since both magnetic and nuclear scattering contribute to the same Bragg peaks it is important to have a large enough q range to refine both contributions simultaneously. Figure 2 shows the NPD pattern and its refinement for the $Rb_yFe_{2-x}Se_2$ sample. For the crystal structure we use the vacancy ordered superstructure model $I4/m$ stated in [8], while for the magnetic structure analysis we use symmetry adapted basis functions of eight irreducible representations (irreps) of the $I4/m$ space group and propagation vector $k = 0$ [8]. The description of the structure model and the magnetic and structure parameters and the details of the refinements are summarized in table 1. It is interesting that in $Cs_yFe_{2-x}Se_2$ the lattice constants a and c have the ratio $(c/a)^2 \simeq 3$, resulting in a complete overlap of the most important Bragg peaks with the magnetic and nuclear contributions, and disentangling the magnetic and crystal structures was possible only using both x-ray and neutron data [8]. For $X_yFe_{2-x}Se_2$ (X = K, Rb) this is not the case, as illustrated in figure 3. The diffraction peaks with the indices groups (101)/(002), (200)/(103) and (211)/(201)/(004) are quite well resolved, whereas in the Cs case they were completely overlapped. Similar to the analysis of $Cs_yFe_{2-x}Se_2$ we have sorted out all irreps (table 3 of [8]) and found that the best fit of our data is achieved for the τ_2 and τ_5/τ_7 irreps for the basis vectors parallel to the c axis (similar to what we have found before for $Cs_yFe_{2-x}Se_2$). The configuration for τ_7 is equivalent to τ_5 after $\pi/2$ rotation around the c axis. Due to better resolution of the magnetic and nuclear contributions and the better statistics of neutron datasets in comparison with $Cs_yFe_{2-x}Se_2$ we are quite confident in the magnetic configurations that we propose. The basis vectors are explicitly listed in [8] and the two magnetic configurations are graphically illustrated in figure 4. The

typo: should be tau3 instead of tau5

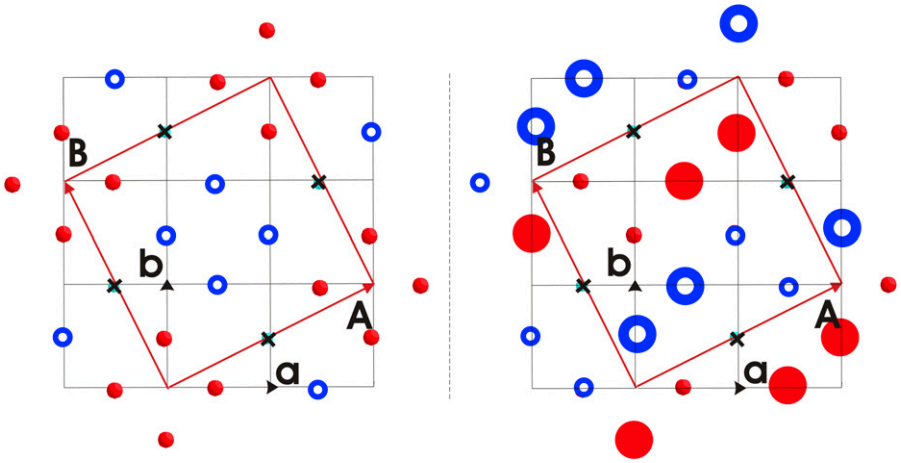

Figure 4. Magnetic configurations for τ_2 (left) and τ_5/τ_7 (right) irreps with the Fe2 magnetic moments along the c axis. Figure shows a projection of one layer of Fe on the (ab) plane. The neighboring planes are arranged antiparallel. Fe1 vacancy positions are shown by the crosses. The τ_5/τ_7 structure can have two different moment sizes indicated by large and small circles. Open blue and filled red circles show Fe2 down and up spins. Large red unit cell (**A**, **B**) corresponds to $I4/m$ cell, while the smaller cells (**a**, **b**) are the cells of the average vacancy disordered $I4/mmm$ (122) structure.

structures with the spins lying in the (ab) plane give considerably ~~better~~ worse reliability factors. For comparison we show the refinement details for τ_4 with the moments in the (ab) plane that gives better R factors among the other 'bad' magnetic models. Besides the poor overall reliability factors the τ_4 structure predicts substantial intensity in the Bragg peak (103), but the experimentally observed intensity is close to zero as shown in figure 3. The magnetic model τ_2 corresponds to the Shubnikov magnetic group $I4/m'$ and gives a constant moment configuration as shown in figure 4, whereas complex τ_7/τ_5 irreps with Herring coefficient 0 do not have a Shubnikov counterpart. In addition, τ_7 gives in general a non-constant moment configuration, as shown in figure 4. The basis function ψ_7 (table 3 of [8]) can be multiplied by an arbitrary phase factor $\exp(i\varphi)$. The overall phase φ does not affect the magnetic Bragg peak intensity at all, because it is proportional to the square of the absolute value of the structure factor $|F|^2$ for unpolarized neutrons. However, the iron moments marked by large and small circles shown in figure 4 will depend on the φ value as $m\cos(\varphi)$ and $m\sin(\varphi)$, where m is the value from table 1. For the constant moment configuration with $\phi = \pi/4$, the moment will be a factor of $\sqrt{2}$ smaller than the maximal m value. In principle, the value of ϕ is accessible in the present $k = 0$ case from the interference term in the polarized neutron diffraction experiment.

Acknowledgments

The authors thank the NCCR MaNEP project and SciexNMS^{ch} (Project Code 10.048) for the support of this study. The work was partially performed at the neutron spallation source SINQ. Fruitful discussions with D Sheptyakov are gratefully acknowledged.

References

[1] Hsu F C *et al* 2008 *Proc. Natl Acad. Sci. USA* **105** 14262
[2] Guo J, Jin S, Wang G, Wang S, Zhu K, Zhou T, He M and Chen X 2010 *Phys. Rev.* B **82** 180520
[3] Krzton-Maziopa A, Shermadini Z, Pomjakushina E, Pomjakushin V, Bendele M, Amato A, Khasanov R, Luetkens H and Conder K 2011 *J. Phys.: Condens. Matter* **23** 052203
[4] Wang A F *et al* 2011 *Phys. Rev.* B **83** 060512
[5] Luo X G *et al* 2011 arXiv:1101.5670
[6] Shermadini Z *et al* 2011 *Phys. Rev. Lett.* **106** 117602
[7] Bao W, Huang Q, Chen G F, Green M A, Wang D M, He J B, Wang X Q and Qiu Y 2011 arXiv:1102.0830
[8] Pomjakushin V Y, Sheptyakov D V, Pomjakushina E V, Krzton-Maziopa A, Conder K, Chernyshov D, Svitlyk V and Shermadini Z 2011 arXiv:1102.1919
[9] Ye F, Chi S, Bao W, Wang X F, Ying J J, Chen X H, Wang H D, Dong C H and Fang M 2011 arXiv:1102.2882
[10] Rotter M, Tegel M and Johrendt D 2008 *Phys. Rev. Lett.* **101** 107006
[11] Häggstrom L, Verma H R, Bjarman S, Wappling R and Berger R 1986 *J. Solid State Chem.* **63** 401–8
[12] Sabrowsky H, Rosenberg M, Welz D, Deppe P and Schafer W 1986 *J. Magn. Magn. Mater.* **54–57** 1497
[13] Haggstrom L, Seidel A and Berger R 1991 *J. Magn. Magn. Mater.* **98** 37
[14] Fang M, Wang H, Dong C, Li Z, Feng C, Chen J and Yuan H Q 2010 arXiv:1012.5236
[15] Wang Z, Song Y J, Shi H L, Wang Z W, Chen Z, Tian H F, Chen G F, Guo J G, Yang H X and Li J Q 2011 arXiv:1101.2059
[16] Zavalij P *et al* 2011 arXiv:1101.4882
[17] Bacsa J, Ganin A Y, Takabayashi Y, Christensen K E, Prassides K, Rosseinsky M J and Claridge J B 2011 arXiv:1102.0488
[18] Fischer P *et al* 2000 *Physica* B **276–278** 146–7
[19] Rodriguez-Carvajal J 1993 *Physica* B **192** 55–69